Materials Today Electronics 9 (2024) 100113

Contents lists available at ScienceDirect

Materials Today Electronics

journal homepage: www.elsevier.com/locate/mtelec

Full Length Article

Material Design and Discovery in Full-Heusler Compounds: A Comprehensive First-Principles Analysis of XMg_2Hg, $XMgHg_2$, and X_2MgHg (X = Sc, Li)

Salman Alsaedi [a], Zahra Nourbakhsh [a,*], Aminollah Vaez [a], Daryoosh Vashaee [b,c,*]

[a] Faculty of Physics, University of Isfahan, Isfahan, Iran
[b] Department of Electrical and Computer Engineering, North Carolina State University, Raleigh, USA
[c] Department of Materials Science and Engineering, North Carolina State University, Raleigh, USA

ARTICLE INFO

Keywords:
Full-Heusler Compounds
First-Principles Calculations
Mechanical Properties
Electronic Properties
Material Stability

ABSTRACT

This study conducts a comprehensive first-principles analysis of the structural, mechanical, phonon dispersion, and electronic properties of XMg_2Hg, $XMgHg_2$, and X_2MgHg (X = Sc and Li) compounds. Using energy-volume curves, cohesive and formation energy, and phonon dispersion analyses, we confirm the stability of these compounds. Our calculations reveal that Li_2MgHg and $ScMg_2Hg$ are more stable in the cubic structure with space group $F\bar{4}3m$ (216), whereas other compounds are stable in the $Fm\bar{3}m$ (225) structure. Phonon dispersion calculations indicate dynamical stability for all compounds except Li_2MgHg in the $Fm\bar{3}m$ structure and Sc_2MgHg and $LiMg_2Hg$ in the cubic structure with space group $F\bar{4}3m$ (216). Mechanical stability is confirmed through the calculation of elastic constants, with Sc-based compounds showing higher bulk modulus, shear modulus, and Young's modulus compared to Li-based compounds. Electronic properties, analyzed through density of states and band structure calculations, confirm the metallic nature of these compounds, with significant contributions from Mg atoms at the Fermi energy. The study also identifies distinct electronic features such as flat electron bands and a Dirac point at the Gamma point for $ScMgHg_2$. Pressure-dependent studies indicate these materials are normal metals without topological phase transitions.

1. Introduction

The search for materials with specific physical properties is a significant focus in materials science. Full-Heusler compounds, represented by the formula X_2YZ, are of particular interest due to their diverse and notable physical properties. These materials typically crystallize in an FCC structure with space groups $F\bar{4}3m$ (216 International number) and $Fm\bar{3}m$ (225 International number). Advances in ab-initio calculation techniques now allow for the prediction of various physical properties of these solids. The substitution of X, Y, and Z atoms in X_2YZ compounds can significantly alter their stable crystal structures and modify their physical properties.

This study investigates the physical properties of XMg_2Hg, $XMgHg_2$, and X_2MgHg (X = Sc and Li) compounds, all of which have a cubic full-Heusler crystal structure. To date, few studies have explored the physical properties of these compounds, and there are no comprehensive theoretical or experimental reports on their stability, mechanical properties, and topological phases. Previous studies indicate that XMg_2Hg, $XMgHg_2$, and X_2MgHg (X = Sc and Li), except Li_2MgHg and $ScMg_2Hg$, are stable in a full-Heusler cubic crystal structure with space group $Fm\bar{3}m$ (225 International number) [1]. Li_2MgHg is stable in the full-Heusler cubic crystal structure with space group $F\bar{4}3m$ (216 International number) [2-4]. However, some reports suggest that Li_2MgHg has a full-Heusler Cu_2MnAl crystal structure with space group $Fm\bar{3}m$ (225 International number) [2-4].

Berland et al. [5] examined the electronic and thermoelectric properties of $MgSc_2Hg$ using density functional theory, finding that it is a promising thermoelectric semiconductor with a small energy band gap of 0.23 eV, suitable for n-type and some p-type applications. Magnesium-based materials are notable for their applications in thermoelectrics, Mg-ion batteries, and optical materials due to their versatile physical properties and structural and chemical flexibility. These materials also enhance corrosion resistance, casting characteristics, and high-temperature mechanical properties [6,7]. Furthermore,

* Corresponding authors.
E-mail addresses: z.nourbakhsh@sci.ui.ac.ir (Z. Nourbakhsh), dvashae@ncsu.edu (D. Vashaee).

https://doi.org/10.1016/j.mtelec.2024.100113
Received 26 May 2024; Received in revised form 3 August 2024; Accepted 10 August 2024
Available online 11 August 2024

magnesium alloys are valued for their low density, excellent machinability, and good stiffness.

Understanding material strength and stability criteria is crucial, and this information can be derived from elastic tensor components [8,9]. Additionally, properties such as bulk modulus, Young's modulus, shear modulus, Poisson's ratio, Pugh's ratio, anisotropic mechanical response, sound velocity, hardness, Debye temperature, and melting point are associated with elastic tensor components [10-12]. Therefore, calculating these components is fundamental to studying the mechanical properties of materials.

The primary objective of this paper is to identify the stable crystal structures and investigate the structural properties of XMg_2Hg, $XMgHg_2$, and X_2MgHg (X = Sc and Li) compounds using total energy-volume curves, formation and cohesive energies, and phonon dispersion calculations. The second objective is to determine the elastic tensor components and examine the mechanical properties of these compounds. The third objective is to analyze the electronic properties, such as linear electronic specific heat, band structure, topological phase, and identifying the topological Dirac point of these compounds.

The paper is organized as follows: Section 2 describes the methods and calculation details. Section 3 explains the results of various physical properties, including structural, mechanical, electronic, and topological phases of these compounds.

2. Method of Calculations

Density functional theory (DFT) is one of the most practical first-principal quantum-mechanical methods for studying the physical properties of many-body particle systems. Numerous codes have been developed for investigating the physical properties of solids using DFT. The Wien2k code [13,14], which is based on DFT and employs the full potential linearized augmented plane wave plus local orbital (APW + lo) method, is widely used for studying the structural, mechanical, and electronic properties of materials. This approach utilizes the APW +lo method to solve the Kohn–Sham equations. Different approximations, such as the generalized gradient approximation (GGA96) [15] using the Perdew–Burke–Ernzerhof scheme, GGA-Engel-Vosko (GGA-EV) [16], and modified Becke-Johnson (mBJ) [17], are employed to obtain the exchange and correlation potentials. The GGA-EV approach, while not suitable for structural calculations, is useful for band structure and energy gap calculations. The structural optimization, stability, structural parameters, elastic tensor components, and mechanical properties of these compounds were calculated using the GGA approach. The electron density of states, linear electronic specific heat, band structures, and topological phases of these compounds were calculated using GGA, GGA-EV, and mBJ approaches. However, due to their close similarity, only the calculated results from the mBJ approach are presented in this work.

In the APW + lo method, each unit cell is divided into non-overlapping muffin-tin spheres and an interstitial region. Spherical harmonics and plane waves are used to expand the Kohn–Sham wave functions, charge density, and crystal potential within the muffin-tin spheres and the interstitial region, respectively. The parameters used in this calculation are as follows: the muffin-tin radii were chosen as $R_{Sc, Mg} = 2.2$ a.u., $R_{Hg} = 2.3$ a.u. and $R_{Li} = 2.1$ a.u. For Brillouin zone integration, 3500 k-points corresponding to a 15 × 15 × 15 mesh in the irreducible wedge were used to achieve self-consistency in solving the Kohn–Sham equations. The cut-off angular momentum quantum number for the expansion of Kohn–Sham wave functions inside the muffin-tin spheres was set to $l_{max} = 10$. The cut-off wave function plane wave expansion in the interstitial region was chosen as as $K_{max} = 9/R_{MT}$ $(a.u.)^{-1}$ (where R_{MT} is the smallest muffin-tin radius in the crystal structure cell). The cut-off for the Fourier expansion of charge density and potential in the interstitial region was set to $G_{max} = 14$ $(Ry)^{1/2}$. These cut-off values and the number of k-points were highly converged with respect to total energy and force at each atomic position, with tolerances of 0.000001 Ry and 0.1 mRy/a.u., respectively.

The elastic constants C_{ij} are crucial for assessing material strength, stability, and safety. These constants are used to determine the mechanical stability of materials. Materials with cubic structures have three independent elastic constants: C_{11}, C_{12}, and C_{44} [18]. Therefore, three equations are needed to determine these independent elastic constants. These equations are obtained by calculating the bulk modulus (B) using the energy-volume curve, performing tetragonal strains to vary the ratio c/a, and applying rhombohedral distortion to vary the length of the cubic diagonal. For the calculation of elastic constants in this work, the IRelast code was used. The IRelast code [19] computes the elastic tensor components for cubic crystal structures using these three equations and the Wien2k self-consistent calculations. The elastic tensor calculations are performed with total energy and force convergence criteria of up to 0.000001 Ry and 0.1 mRy/a.u. at each atomic position, respectively.

The Born-Huang criterion is a useful approach for evaluating the mechanical stability of crystal structures [20]. For cubic crystal lattices, the Born-Huang criterion is given by:

$$C_{11} - C_{12} > 0,\ C_{11} + 2C_{12} > 0,\ \ C_{44} > 0 \tag{1}$$

Mechanical properties can be calculated using the elastic constants. For the calculation of mechanical properties analysis using the elastic tensor components, the ElaTools code [21] was employed. ElaTools code calculates the mechanical properties including bulk modulus (B_V, B_R and B_{VRH}), Young's modulus (E_V, E_R and E_{VRH}), shear modulus (G_V, G_R and G_{VRH}), Poisson's ratio (ν_V, ν_R and ν_{VRH}), Pugh's ratio (B/G) within Voigt, Reuss and Voigt-Reuss-Hill (VRH) average approximations [22-24] as follow:

$$G_V = \frac{1}{5}(3c_{44} + c_{11} - c_{12}),\ G_R = \frac{5(c_{11} - c_{12})c_{44}}{4c_{44} + (c_{11} - c_{12})},\ G_{VRH} = \frac{(G_V + G_R)}{2},$$
$$B_V = B_R = \frac{C_{11} + 2C_{12}}{3} \tag{2}$$

Furthermore, the universal anisotropy index (A^U), Zener anisotropy factor (A^Z) and the Kube's log-Euclidean anisotropy (A^L), which describe elastic anisotropy are calculated as follow [25-27]:

$$A^U = 5\frac{G_V}{G_R} + \frac{B_V}{B_R} - 6,\ A^Z = 2\frac{C_{44}}{C_{11} - C_{12}} \tag{3}$$

$$A^L = \sqrt{\ln\left(\frac{B_V}{B_R}\right)^2 + 5\ln\left(\frac{G_V}{G_R}\right)^2} \tag{4}$$

where G_R and B_R (G_V and B_V) are the shear and bulk moduli using the Reuss (Voigt) approximation respectively.

Using the calculated bulk modulus and shear modulus within Voigt, Reuss and Voigt-Reuss-Hill average approximations. The Young's modulus (E) and Poisson's ratio can be calculated as follow [28]:

$$E = \frac{9BG}{3B + G} \tag{5}$$

$$\upsilon = \frac{3B - 2G}{6B + 2G} \tag{6}$$

Phonon dispersions describe the dynamical stability of materials. For phonon dispersion calculations of these compounds, the Phonopy code [29] was used. This code treats atomic vibrations with small displacements using second-order terms, and higher-order terms (anharmonic scattering) are calculated using perturbation theory. In this work, phonon dispersion calculations were performed using a 2 × 2 × 2 supercell with 32 atoms and 16 displacements. Additionally, the total energy and force at each atomic position were highly converged up to 0.00001 Ry and 0.1 mRy/a.u., respectively. The self-consistent

calculations for each displacement were conducted using first-principles calculations based on density functional theory within the GGA approach in the Wien2k package.

3. Results and discussion

3.1. Structural properties

To determine the stable crystal structures of XMg_2Hg, $XMgHg_2$, X_2MgHg (X = Sc and Li) compounds, we calculated the total energy for different volumes of these compounds in both ferromagnetic and nonmagnetic phases, with and without spin-orbit interaction, using the GGA approach. These calculations were performed for two cubic crystal structures with space groups $Fm\bar{3}m$ (225) and $F\bar{4}3m$(216). These results were fitted using the Birch-Murnaghan equation of state. The calculations indicate that XMg_2Hg, $XMgHg_2$, X_2MgHg (X=Sc and Li) compounds are nonmagnetic, showing no magnetic order.

Fig. 1 presents the calculated total energy versus volume for these

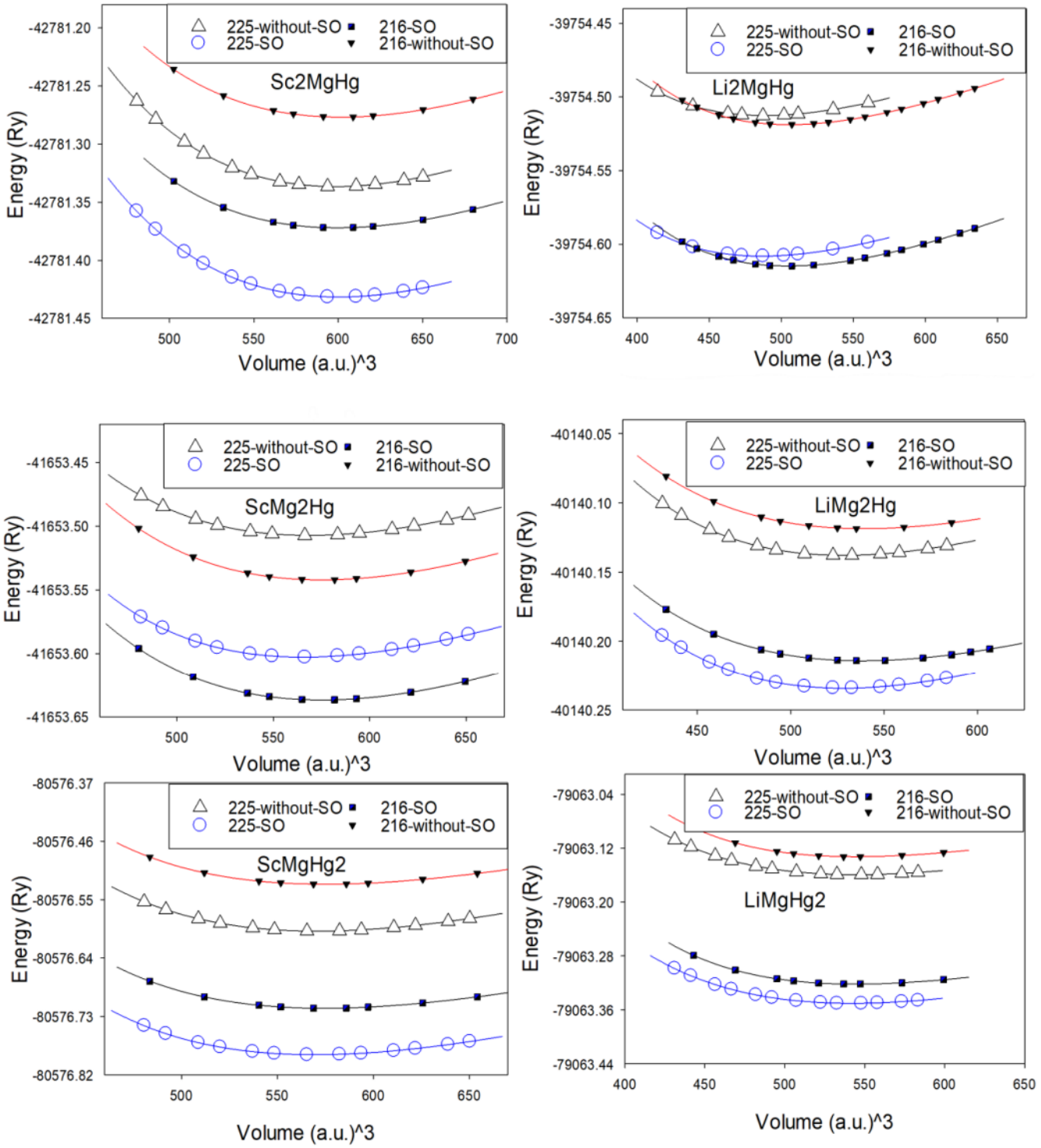

Fig. 1. The calculated total energy versus volume for XMg_2Hg, $XMgHg_2$, and X_2MgHg (X = Sc and Li) compounds, in both the presence and absence of spin-orbit interaction within GGA approach, in the nonmagnetic phase. Results are shown for two different cubic structures: $Fm\bar{3}m$ (225) and $F\bar{4}3m$(216) space groups.

compounds in both cubic structures, with and without spin-orbit interaction within the GGA approach. The results indicate that Li_2MgHg and $ScMg_2Hg$ are more stable in the cubic structure with space group $F\bar{4}3m(216)$, while the other compounds are more stable in the cubic structure with space group $Fm\bar{3}m$ (225). These findings align with previously reported results [1]. Additionally, Fig. 1 shows that the Li_2MgHg compound undergoes a transition from the cubic structure with space group $F\bar{4}3m(216)$ to $Fm\bar{3}m$ (225) at 5.19 GPa.

The calculated lattice parameters, bulk modulus, and minimum energy of these compounds, with and without spin-orbit interaction in both cubic structures, are provided and compared with available reported results in Table 1. Spin-orbit interaction has a negligible effect on the lattice parameters and bulk modulus but significantly impacts the energy-volume diagram (Fig. 1), highlighting its importance. Comparison with other results demonstrates that these calculations are in good agreement with previously reported findings [1].

The unit cell volume of each compound is proportional to the atomic size and the bonding of adjacent atoms in the solid. Due to the different atomic sizes of Sc and Li, the calculated lattice parameters of XMg_2Hg, $XMgHg_2$, and X_2MgHg compounds with X = Sc are larger than those for X = Li. The bulk moduli of materials are related to the degree of covalency and ionicity. Generally, the bulk modulus increases with covalency and decreases with ionicity due to bonding charge reduction. The calculated bulk modulus for compounds with X = Sc is larger than for X = Li, attributed to the decrease in covalency and increase in ionicity when Sc is replaced by Li.

To investigate the stability of XMg_2Hg, $XMgHg_2$, X_2MgHg (X=Sc and Li) compounds, we studied the enthalpy of formation (ΔH_f) and cohesive energy (E_C). The cohesive energies (E_C) of X_2YZ compounds are calculated using the following equation [30-32]:

$$E_C = \frac{E_{Bulk}^{total}(X_2YZ) - N_X E_X^{total} - N_Y E_Y^{total} - N_Z E_Z^{total}}{N_X + N_Y + N_Z} \quad (7)$$

where $E_{Bulk}^{total}(X_2YZ)$ is the total energy per formula unit of X_2YZ bulk, E_X^{total}, E_Y^{total}, and E_Z^{total} are the total energies of individual X, Y, and Z atoms. N_X, N_Y, and N_Z are the number of X, Y, and Z atoms in the unit cell. The formation energies ΔH_f) of X_2YZ compounds are calculated using [30-32]:

$$\Delta H_f(X_2YZ) = E^{total}(X_2YZ) - 2E^{total}(X) - E^{total}(Y) - E^{total}(Z) \quad (8)$$

where $E^{total}(X_2YZ)$ is the total energy per formula unit of the X_2YZ compound, and $E^{total}(X)$, $E^{total}(Y)$ and $E^{total}(Z)$ are the total energies per atom of pure X, Y, and Z elements in their stable crystal structures.

The calculated cohesive and formation energies of these compounds, with and without spin-orbit interaction within the GGA approach in both cubic structures, are given and compared with available reported results [1] in Table 2. The negative cohesive and formation energies indicate structural stability. The results show that the cohesive and formation energies of these compounds in their stable phases are lower than in other phases. The most stable crystal structures of these compounds, as determined from cohesion and formation energy calculations, correspond to the results obtained from the energy-volume diagram.

For the dynamical stability of each material, it is necessary that all phonon frequencies are positive. Therefore, any phonon density of states with negative frequencies, which correspond to imaginary phonon frequencies, indicates the dynamical instability of materials. To study the dynamical stability, the phonon dispersion and partial phonon density of states of these compounds were calculated using the full-potential Wien2k package and the Phonopy code [29] for a 2 × 2 × 2 supercell within the GGA approach. The calculated partial phonon density of states of these compounds in cubic structures with $Fm\bar{3}m$ (225) and $F\bar{4}3m(216)$ space groups is shown in Fig. 2 and 3, respectively.

There are no imaginary phonon frequencies in XMg_2Hg, $XMgHg_2$ and X_2MgHg (X = Sc and Li) compounds in cubic structures with $Fm\bar{3}m$ (225), except for the Li_2MgHg compound, indicating the dynamical stability of these compounds and their potential for laboratory synthesis. However, XMg_2Hg, $XMgHg_2$ and X_2MgHg (X = Sc and Li) compounds in

Table 1
The calculated lattice parameters (a(Å)), bulk modulus (B(GPa)) and minimum energy ($E_0(Ry)$) for one formula unit of these compounds within GGA approach in the presence and absence of spin-orbit interaction in two different cubic structures with $Fm\bar{3}m$ (225) and $F\bar{4}3m$ (216) space groups, and available reported results [1].

Compounds	Reference	Space Group	Spin-Orbit Interaction	a (Å)	B (GPa)	E_0(Ry)
$ScMgHg_2$	This work	$F\bar{4}3m$ (216)	Yes	6.9817	60.59	-80576.7174
			No	6.9848	58.87	-80576.5263
		$Fm\bar{3}m$ (225)	Yes	6.9624	67.69	-80576.7890
			No	6.9672	66.69	-80576.5985
	[1]			6.90	——-	———
$ScMg_2Hg$	This work	$F\bar{4}3m(216)$	Yes	6.9854	55.39	-41653.6367
			No	6.9848	54.78	-41653.5421
		$Fm\bar{3}m$ (225)	Yes	6.9439	54.74	-41653.6027
			No	6.9598	50.26	-41653.5072
				——-	——-	———
Sc_2MgHg	This work	$F\bar{4}3m(216)$	Yes	7.0830	54.33	-42781.3719
			No	7.0910	54.42	-42781.2767
		$Fm\bar{3}m$ (225)	Yes	7.0854	62.41	-42781.4314
			No	7.0787	63.66	-42781.3364
	[1]			7.05	——-	——-
$LiMg_2Hg$	This work	$F\bar{4}3m$ (216)	Yes	6.8331	35.79	-40140.2141
			No	6.8372	35.72	-40140.1186
		$Fm\bar{3}m$ (225)	Yes	6.7902	44.30	-40140.2342
			No	6.7911	42.55	-40140.1379
	[1]			6.71	43	——-
$LiMgHg_2$	This work	$F\bar{4}\bar{3}m$ (216)	Yes	6.8586	42.33	-79063.3217
			No	6.8592	41.27	-79063.1326
		$Fm\bar{3}m$ (225)	Yes	6.8500	44.69	-79063.3503
			No	6.8602	40.1192	-79063.1591
	[1]			6.76	——	——
Li_2MgHg	This work	$F\bar{4}3m(216)$	Yes	6.6885	34.23	-39754.61479
			No	6.6909	33.57	-39754.5187
		$Fm\bar{3}m$ (225)	Yes	6.6058	31.81	-39754.6080
			No	6.6146	30.74	-39754.5125
	[1]			6.61	——-	——

Table 2
The calculated cohesive and formation energies of these compounds within GGA approach in the presence and absence of spin-orbit interaction in two different cubic structures with space groups $Fm\bar{3}m$ (225) and $F\bar{4}3m$(216) and the available data in the literature [1].

Space Group		Spin-Orbit Interaction	$LiMgHg_2$	$LiMg_2Hg$	Li_2MgHg	$ScMgHg_2$	$ScMg_2Hg$	Sc_2MgHg
Cohesive energy (eV/atom) (This work)	$F\bar{4}3m$(216)	Yes	-1.920	-2.128	-3.492	-1.152	-11.744	-1.44
		No	-1.196	-1.800	-2.612	-0.504	-11.420	-1.968
	$Fm\bar{3}m$ (225)	Yes	-1.940	-2.196	-2.916	-1.396	-11.628	-2.860
		No	-1.288	-1.864	-2.520	-0.748	-11.304	-2.212
Formation energy (eV/atom) (This work)	$F\bar{4}3m$(216)	Yes	-0.388	-0.356	-0.564	-0.196	-0.260	-0.068
		No	0.2560	-0.032	-0.236	0.452	0.064	0.252
	$Fm\bar{3}m$ (225)	Yes	-0.484	-0.424	-0.540	-0.440	-0.144	-0.272
		No	0.164	-0.100	-0.216	0.208	0.180	0.052
Literature [1]			-0.300	-0.241	-0.270	-0.377	——	-0.232

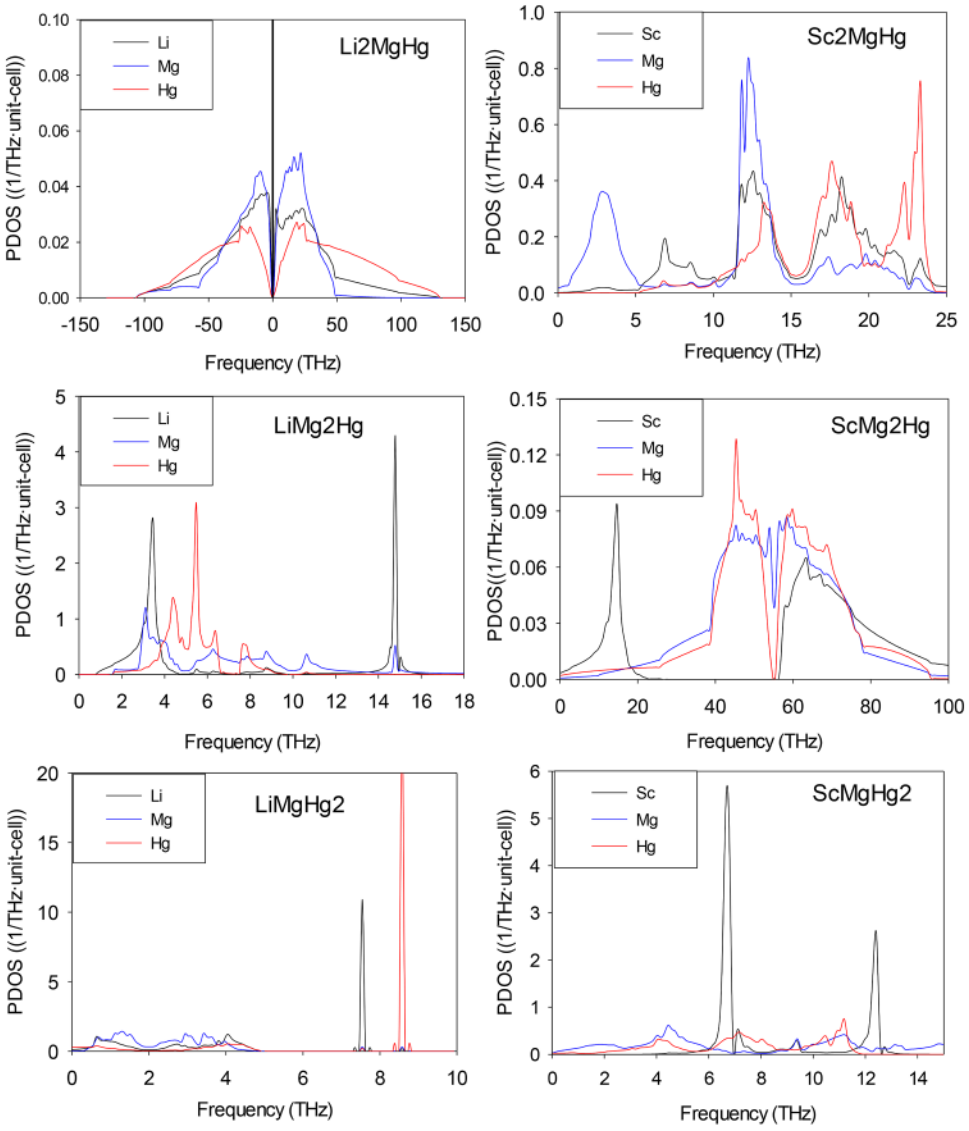

Fig. 2. The calculated phonon density of stats (PDOS) of XMg_2Hg, $XMgHg_2$, and X_2MgHg (X = Sc and Li) compounds in cubic structures with $Fm\bar{3}m$ (225) space group, in the presence of spin-orbit interaction within GGA approach.

cubic structures with $F\bar{4}3m$(216), except for LiMg2Hg and Sc2MgHg, exhibit phonon distributions with negative frequencies, indicating dynamical instability. The presence of imaginary phonon frequencies can be attributed to factors such as atomic number, chemical bonding, and atomic position geometry, including atomic arrangement and crystal structure symmetry.

3.2. Elastic properties

The calculated elastic tensor components of the XMg_2Hg, $XMgHg_2$, X_2MgHg (X=Sc and Li) compounds in their stable crystal structures within GGA approach are presented in Table 3. These components satisfy the Born-Huang criterion, indicating that these materials are mechanically stable.

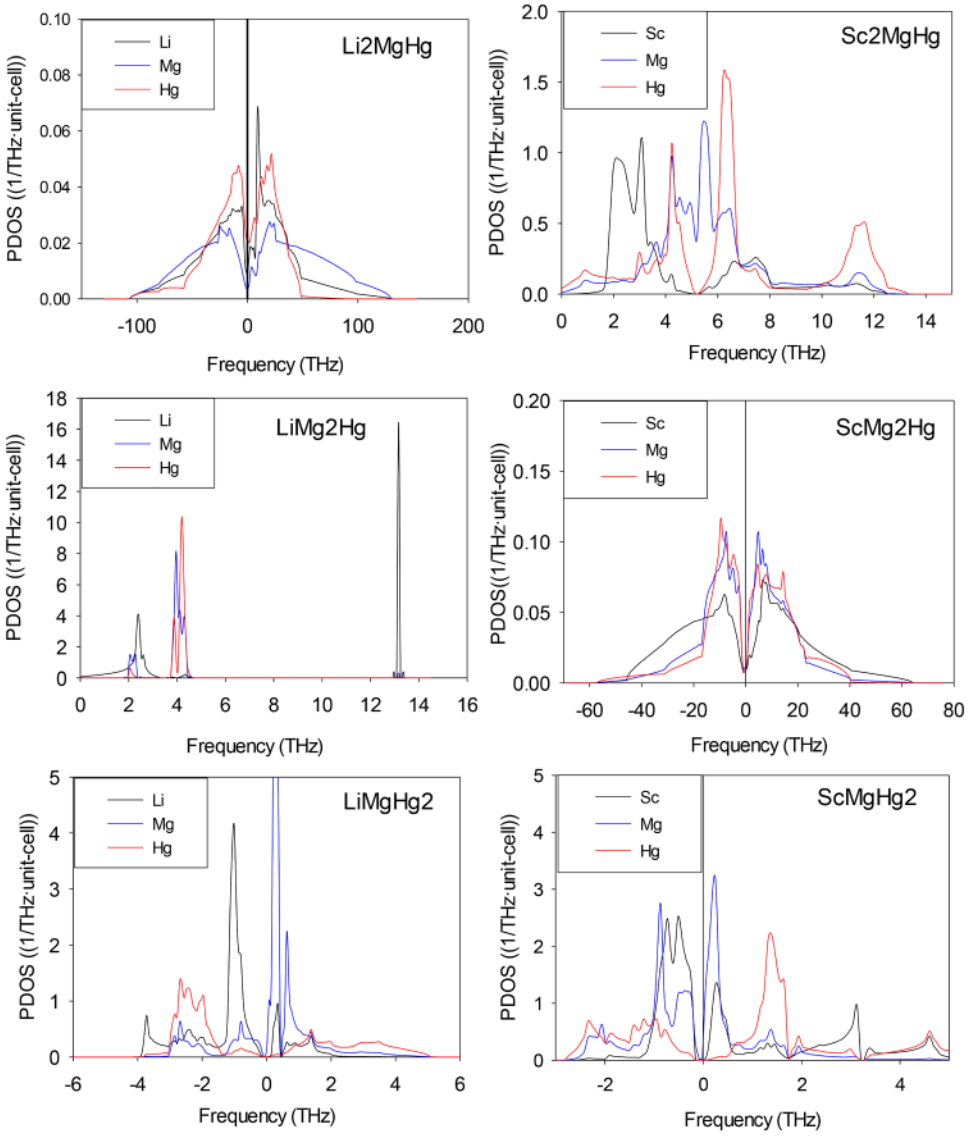

Fig 3. The calculated phonon density of stats (PDOS) of XMg_2Hg, $XMgHg_2$, and X_2MgHg (X = Sc and Li) compounds in cubic structures with $F\bar{4}3m$(216) space group, in the presence of spin-orbit interaction within GGA approach.

Table 3
The calculated elastic constants (C_{ij}) and Cauchy pressure (P_C) of Xg_2Hg, $XMgHg_2$, X_2MgHg (X=Sc and Li) **compounds** within GGA approach in the presence of spin-orbit interaction.

	$LiMgHg_2$	$LiMg_2Hg$	Li_2MgHg	$ScMgHg_2$	$ScMg_2Hg$	Sc_2MgHg
C_{11}(GPa)	60.80	63.50	43.22	90.54	72.43	83.63
C_{12} (GPa)	36.46	34.78	30.41	56.93	47.59	52.83
C_{44} (GPa)	35.95	49.01	37.11	50.50	52.13	65.18
$C_{11} - C_{12}(GPa)$	24.34	28.72	12.81	33.61	24.84	30.80
$P_C = C_{12} - C_{44}$	24.85	14.49	6.11	6.43	20.30	18.45

The C_{11} component of the elastic tensor represents the material's resistance to linear compression in the [100] direction [18], while the C_{44} component indicates the material's resistance to monoclinic shear stress in the [001] direction on the (100) plane [18,33]. The results show that the C_{11} component is larger than the C_{12} and C_{44} components, suggesting that these compounds are more resistant to compression along the [100] direction, indicating stronger atomic bonding in this direction.

Some fundamental mechanical properties, such as bulk modulus (B_V, B_R and B_{VRH}), Young's modulus, shear modulus, Poisson's ratio, Pugh's ratio within Voigt, Reuss and Voigt-Reuss-Hill (VRH) average approximations, universal anisotropy index, Zener anisotropy factor, and the Kube's log-Euclidean anisotropy [22,23] are calculated and presented in Table 4.

The response of materials to compressibility due to hydrostatic pressure depends on the bulk modulus (B) [18]. The bulk modulus also indicates the strength of atomic bonds in crystals. The bulk modulus of these compounds, previously calculated using the total energy-volume

Table 4
The calculated elastic constants bulk modulus (B_V, B_R *and* $B_{Average}$), Young's modulus ((E_V, E *and* $E_{Average}$)), shear modulus (G_V, G_R *and* $G_{Average}$)), Poisson's ratio (ν_V, ν_R *and* $\nu_{Average}$), Pugh's ratio (B/G) within Voigt's and, Reuss's approximations, universal anisotropy index (A^U), Zener anisotropy factor (A^Z), and the Kube's log-Euclidean anisotropy (A^L) of XMg_2Hg, $XMgHg_2$, X_2MgHg (X=Sc and Li) compounds within GGA approach in the presence of spin-orbit interaction using Voigt, Reuss, and Voigt-Reuss-Hill approximations.

			$LiMgHg_2$	$LiMg_2Hg$	Li_2MgHg	$ScMgHg_2$	$ScMg_2Hg$	Sc_2MgHg
Bulk modulus (GPa)	B_V		44.58	44.35 43 [1]	38.02	68.13	53.83	63.09
	B_R		44.58	44.35 43 [1]	38.02	68.13	53.83	63.09
	B_{VRH}		44.58	44.35	38.02	68.13	53.83	63.09
Shear modulus (GPa)	G_V		31.62	35.16 30 [1]	26.83	37.02	31.09	45.27
	G_R		21.58	24.94 15 [1]	19.51	28.02	16.38	28.43
	G_{VRH}		26.60	30.05	23.17	32.52	23.73	36.85
Young modulus (GPa)		E_V	76.72	83.43	65.16	94.03	78.22	109.61
		E_R	55.75	63.01	49.98	73.93	75.67	74.15
		E_{VRH}	66.56	73.53	57.77	84.17	62.08	92.53
Poisson ratio		ν_V	0.21	0.19 0.27 [1]	0.21	0.27	0.26	0.21
		ν_R	0.29	0.26	0.28	0.31	0.36	0.30
		ν_{VRH}	0.25	0.22	0.24	0.29	0.31	0.25
Pugh's ratio (B/G)		$(B/G)_V$	1.4099	1.26	1.42	1.84	1.7313	1.3937
		$(B/G)_R$	2.0657	1.78	1.95	2.43	3.2876	2.2196
		$(B/G)_{VRH}$	1.6759	1.48	1.64	2.09	2.2682	1.7122
Universal anisotropy index (A^U)			2.3259	2.0479 5.04 [1]	1.8759	1.6054	4.4946	2.9632
Zener anisotropy factor (A^Z)			3.6654	3.4136	3.2561	3.0051	5.5658	4.2131
Zener anisotropy factor (A^L)			0.8541	0.7676	0.7124	0.6226	1.4340	1.0407

curve (in Section 3.1), is recalculated using the elastic tensor components. The results are consistent with those from Section 3.1. Comparing the results in Table 4 shows that the bulk modulus of Sc-based compounds is larger than that of Li-based compounds, indicating that Li-based compounds are more compressible and have weaker bond strengths.

The shear modulus, equal to the ratio of shear stress to shear strain, indicates the solid's rigidity. It is a critical parameter for evaluating deformation resistance and hardness under shear stress [33,34]. The shear modulus of these compounds is of the same order of magnitude, with Sc_2MgHg having a slightly larger value than the other compounds.

Young's modulus, the ratio of stress (force per unit area $\sigma = F/A$) to strain (extension per unit length $\varepsilon = dl/l$), is used to determine solid stiffness. A larger Young's modulus indicates a stiffer solid [24]. The calculated Young's modulus for XMg_2Hg, $XMgHg_2$, X_2MgHg compounds with X = Sc is larger than for X = Li. Additionally, Sc_2MgHg and Li_2MgHg have the highest and lowest stiffness, respectively.

The Sc_2MgHg (Li_2MgHg) compound has larger (smaller) values of Young's modulus and shear modulus compared to the other compounds, indicating a higher (lower) degree of resistance to deformation, hardness, and stiffness. The calculated shear modulus and Young's modulus of these compounds are almost of the same order as those of aluminum alloys, which are 26.91 GPa and 70 GPa, respectively [35].

Poisson's ratio (ν) and Pugh's ratio (B/G) are important for describing material ductility and brittleness. Poisson's ratio also can describe the stability of materials under shear deformation [36]. A Poisson's ratio of 0.26 and a Pugh's ratio of 1.75 are criteria distinguishing ductile from brittle materials. Materials with $B/G > 1.75$ and $\nu > 0.26$ are ductile; otherwise, they are brittle [37]. The results in Table 4 show $ScMgHg_2$ and $ScMg_2Hg$ are ductile, while the other compounds are brittle. A Poisson's ratio of around 0.25 indicates materials dominated by ionic contributions, while lower values suggest covalent bonding. The average Poisson's ratios, except for $ScMg_2Hg$, $ScMgHg_2$ and $LiMg_2Hg$, are about 0.25, implying that interatomic forces in these compounds are primarily ionic.

In addition to, Cauchy pressure (P_C), defined as $P_C = C_{12} - C_{44}$ describes the brittleness and ductility of solids [38-40]. The Cauchy pressure critical value is zero, which separates the materials with ductile and brittle bonds. Materials with negative P_C are covalent with brittle bonds, while positive P_C indicates metallic-like ductility bonding with delocalized electrons. Cauchy pressure of these compounds is calculated and also given in Table. 3. The positive P_C values for these compounds suggest metallic-like ductility bonding.

Elastic anisotropy shows the material response to strain in all directions and is an important mechanical property [41]. Anisotropic mechanical response to external stress can be studied using anisotropy indices. A crystal with $A^U = 0$ and $A^Z = 1$ is isotropic, while deviations indicate anisotropy. The degree of anisotropy is represented by the departure of A^U and A^Z from zero and one, respectively. The calculated anisotropy indices (A^U and A^Z) for XMg_2Hg, $XMgHg_2$, X_2MgHg (X=Sc and Li) compounds are given in Table 4. $ScMg_2Hg$ and $ScMgHg_2$ have the largest and smallest deviations, respectively, indicating significant differences in elastic anisotropy. Materials with $A^L = 0$ are elastically isotropic. The calculated A^U, A^Z and A^L indicate that $ScMg_2Hg$ has more anisotropy, while $ScMgHg_2$ has less.

Furthermore, the three-dimensional surface structure of Young's modulus is a useful indicator of a material's elastic anisotropy. For elastically isotropic materials, the three-dimensional surface of Young's modulus is spherical, and its projection on different planes is circular. Deviations from spherical or circular shapes indicate the degree of elastic anisotropy.

Using the ELATOOLS package, we calculated the three-dimensional surface structures and their xy-plane projections of Young's modulus for the compounds studied. These results are shown in Fig. 4 and 5. The three-dimensional surface structures of Young's modulus for these compounds deviate from spherical symmetry, indicating elastic anisotropy. Among the compounds, $ScMg_2Hg$ exhibits the largest deviation from spherical symmetry, while $ScMgHg_2$ shows the smallest deviation.

The projection of Young's modulus in the xy-plane for XMg_2Hg, $XMgHg_2$, X_2MgHg (X=Sc and Li) compounds in their equilibrium crystal structure phases further illustrates their anisotropic properties. The deviation of these projections from circular symmetry is consistent with the three-dimensional surface structures and the calculated universal anisotropy indices. Specifically, the projections for $ScMg_2Hg$ and $ScMgHg_2$ exhibit the largest and smallest deviations from circular

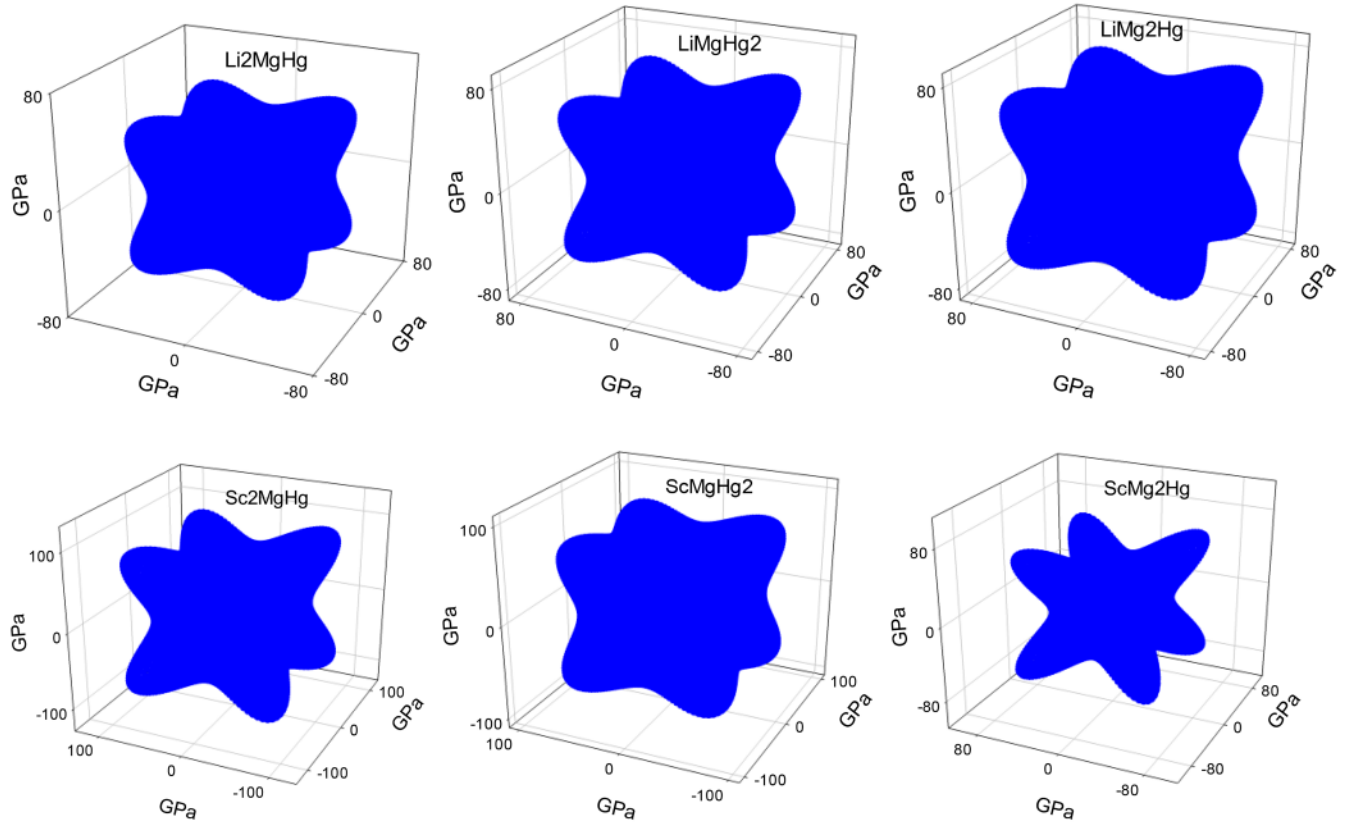

Fig. 4. Three-dimensional surface representation of Young's modulus for XMg_2Hg, $XMgHg_2$, and X_2MgHg (X = Sc and Li) compounds within GGA approach in the presence of spin-orbit interaction in their equilibrium crystal structure phase

symmetry, respectively, confirming their respective degrees of elastic anisotropy.

3.3. Electronic properties

3.3.1. Electron density of states

To investigate the electronic properties of XMg_2Hg, $XMgHg_2$, and X_2MgHg (X=Sc and Li) compounds, we calculated the electron density of states (DOS) within GGA, GGA-EV and mBJ approaches in their stable crystal structure phases. Due to similar behaviors of the calculated results within the GGA, GGA-EV and mBJ approaches, only the results from the mBJ approach are shown in Fig. 6. The results indicate that these compounds are metallic, with the main distribution of the electron density of states at the Fermi energy primarily attributed to the Mg atom. Using the calculated electron density of states at the Fermi energy, we calculated the linear electronic specific heat of these compounds using the following equation:

$$\gamma = \frac{\pi^2}{3} K_B^2 D(E_F) \quad (9)$$

where γ, K_B and $D(E_F)$ are the linear electronic specific heat, Boltzmann constant, and the electron density of states at the Fermi energy, respectively. The calculated linear electronic specific heat per formula unit of these compounds within the mBJ approach, with and without spin-orbit coupling, is provided in Table 5. The results show that the linear electronic specific heat of XMg_2Hg, $XMgHg_2$, and X_2MgHg compounds with X = Sc is larger than the corresponding values for X = Li.

To understand the effect of pressure on the linear electronic specific heat of these compounds, we calculated the total and partial contributions of Sc, Li, Mg, and Hg atoms to γ at different pressures. The results are shown in Fig. 7. In all compounds, except Sc_2MgHg, the linear electronic specific heat exhibits an almost linear behavior with slight variation and decreases with increasing pressure. The results indicate that Sc and Li atoms have the highest and lowest contributions to the linear electronic specific heat, respectively.

The different behavior of the linear electronic specific heat of Sc_2MgHg under pressure compared to other compounds is due to the presence of a Sc atom peak near the Fermi energy. This peak shifts towards and eventually aligns with the Fermi energy at approximately 12.5 GPa, resulting in a distinct change in the electronic specific heat behavior under pressure.

3.3.2. Band structure

The band structures of XMg_2Hg, $XMgHg_2$, and X_2MgHg (X=Sc and Li) compounds were calculated using GGA, GGA-EV, and mBJ approaches in their stable crystal structure phases, both with and without spin-orbit coupling. Due to the similar behavior observed in the calculated band structures across these methods, only the mBJ results with spin-orbit coupling are shown in Fig. 8. The results indicate that all these compounds are metallic.

The band structures of Sc_2MgHg, $ScMg_2Hg$ and $ScMgHg_2$ share some common features. Notably, several electron bands around the Fermi energy are flat in the L-X direction and dispersive in the W-L and X-K directions. A Dirac point with a band opening of 0.024 eV is present at the Gamma point in the band structure of $ScMgHg_2$. In contrast, the band structures of Li_2MgHg, $LiMg_2Hg$ and $LiMgHg_2$ exhibit more dispersive characteristics around the Fermi energy. The band structure similarities between $ScMg_2Hg$ and $LiMg_2Hg$, and between $ScMgHg_2$ and $LiMgHg_2$, are more pronounced than those between Sc_2MgHg and Li_2MgHg. This difference arises from the distinct electronic structures of Sc and Li atoms. Due to the presence of a Dirac point, the electrical conduction of $ScMgHg_2$ can be described by massless fermions as charge carriers. These massless fermions give rise to various phenomena, including quantum Hall effects, magnetoelectric effects, and ultra-high

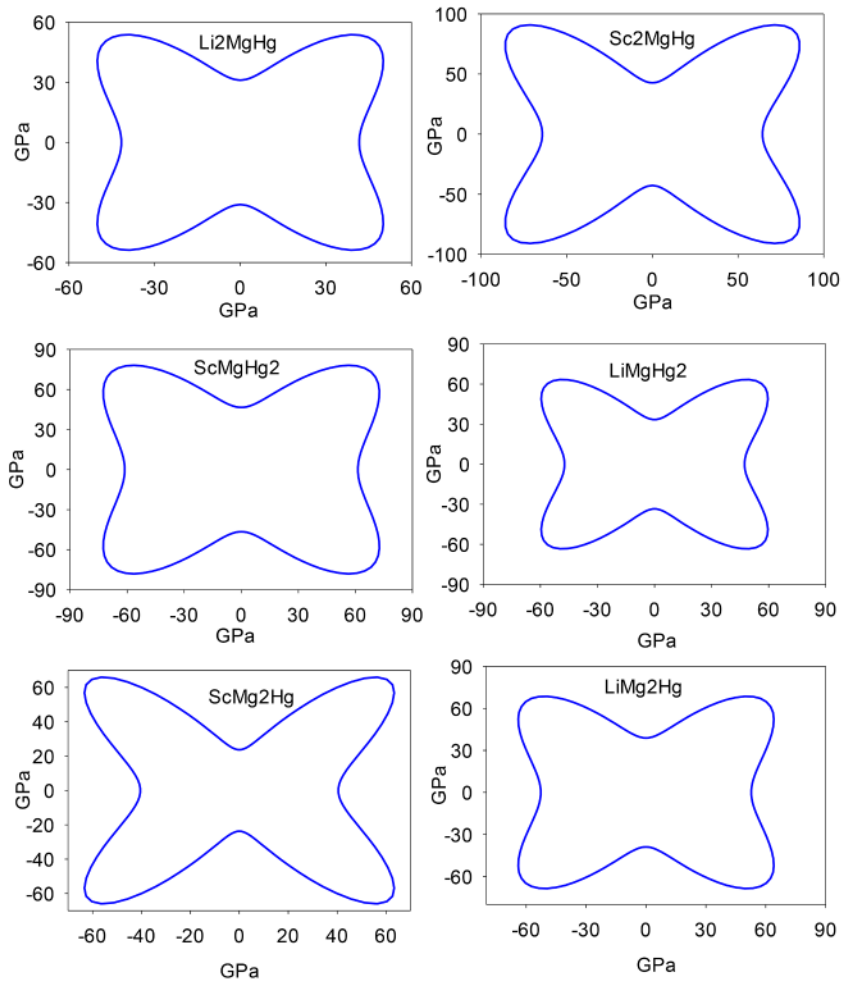

Fig 5. The projection of Young's modulus in the xy-plane for XMg_2Hg, $XMgHg_2$, and X_2MgHg (X = Sc and Li) compounds within GGA approach in the presence of spin orbit interaction in their equilibrium crystal structure phase.

carrier mobility.

To investigate the topological inversion and band order of these compounds, we analyzed the distribution of s, p, and d electrons in the band structure with spin-orbit coupling under different pressures (ranging from -7 GPa to 10 GPa). The results show that these compounds exhibit normal band order without any band inversion within the studied pressure range. Therefore, these compounds are normal metals and do not undergo any topological phase transitions.

3.3.2.1. Potential Applications of XMg_2Hg, $XMgHg_2$, and X_2MgHg Compounds. Based on the results obtained in this study, the XMg_2Hg, $XMgHg_2$, and X_2MgHg (X = Sc and Li) compounds show promising potential for various applications across different fields. These materials, being part of the Heusler compound family, have inherent properties that make them attractive for spintronic devices due to their unique transport properties and potential for high spin polarization [42]. The metallic nature and significant contributions from Mg atoms at the Fermi energy suggest these compounds could be useful in electronic applications where tunable conductivity is desired.

The mechanical stability and elastic properties of these compounds, particularly the higher stiffness of Sc-based compounds, indicate potential uses in structural applications where lightweight yet strong materials are required. This aligns with the general advantages of magnesium alloys in industries such as automotive, aerospace, and defense, where weight reduction is crucial [43].

Furthermore, the presence of a Dirac point in $ScMgHg_2$ could be exploited in quantum electronic devices or topological insulators. These materials could be used in developing new quantum computing technologies or advanced electronic components that leverage the unique properties of Dirac fermions. The pressure-dependent studies showing these materials remain normal metals without topological phase transitions suggest they could be used in high-pressure environments without significant property changes.

In the realm of energy applications, while not explicitly studied in this work, many Heusler compounds, especially half-Heuslers, have shown promise as thermoelectric materials [44]. The ability to tune the electronic properties of these compounds through composition adjustments could potentially lead to optimized thermoelectric performance for energy harvesting or cooling applications.

Lastly, the biocompatibility of magnesium-based materials suggests that, with proper surface treatment to address corrosion issues, these compounds could find applications in biomedical engineering, such as in temporary implants or drug delivery systems [45]. However, further studies on biocompatibility and long-term stability would be necessary to fully explore this potential application area.

4. Conclusions

This study has investigated the structural, mechanical, electronic, and topological properties of XMg_2Hg, $XMgHg_2$, and X_2MgHg (X = Sc and Li) compounds with a cubic full-Heusler crystal structure. Our findings indicate that these compounds are nonmagnetic and exhibit structural stability, as confirmed by their cohesive and formation energies. Li_2MgHg and $ScMg_2Hg$ are more stable in the cubic structure

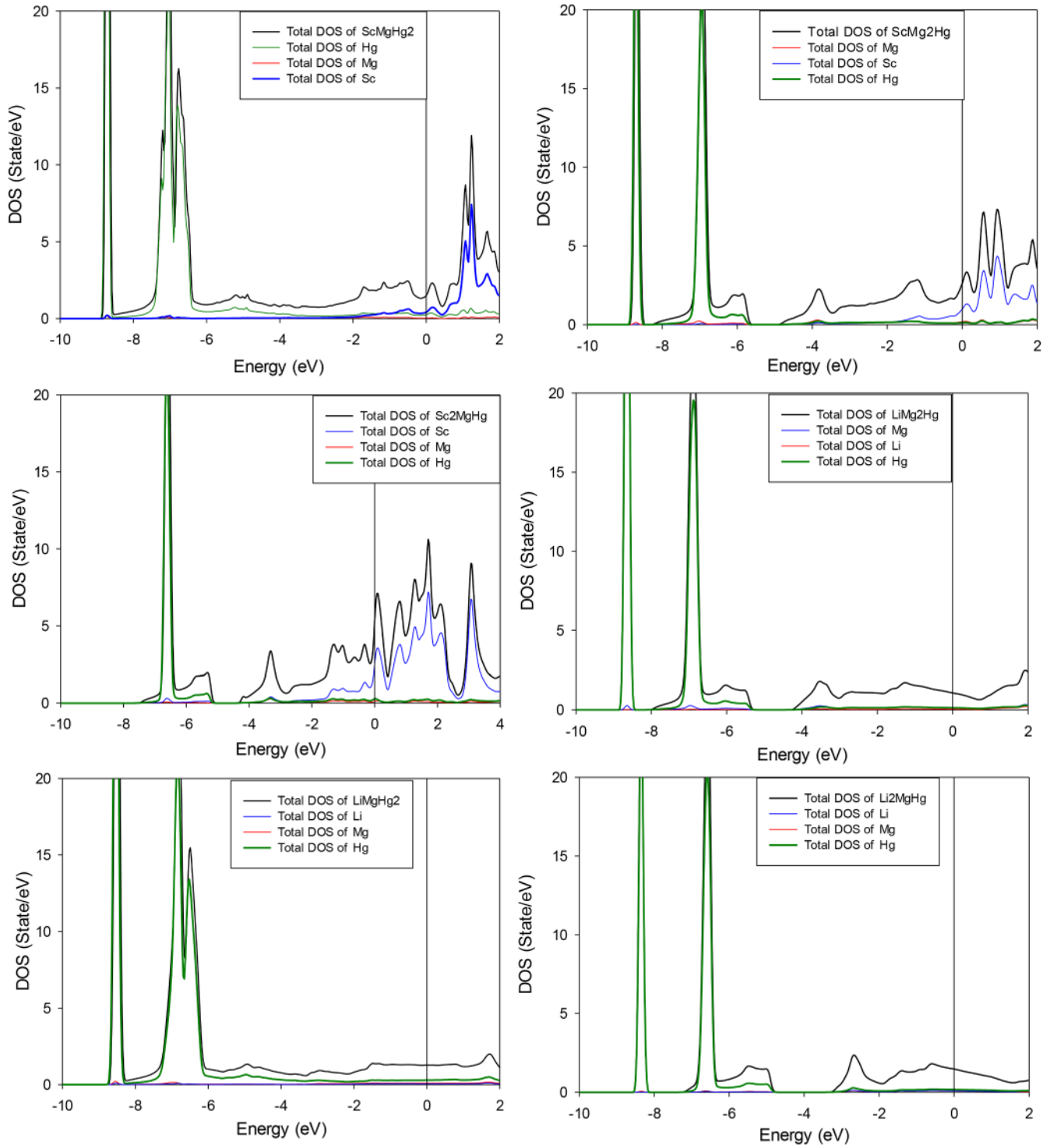

Fig. 6. The calculated total and partial density of states (DOS) for MMg_2Hg, $MMgHg_2$, and M_2MgHg (M = Sc and Li) compounds within mBJ approach in the presence of spin- orbit interaction.

Table 5
The calculated linear electronic specific heat (γ) of these compounds within mBJ approach in the presence of spin-orbit interaction

$\gamma\left(mJmol^{-1}K^{-2}\right)$	$LiMgHg_2$	$LiMg_2Hg$	Li_2MgHg	$ScMgHg_2$	$ScMg_2Hg$	Sc_2MgHg
With SOI	3.02	2.50	3.46	3.51	4.70	11.03
Without SOI	2.96	2.50	3.48	3.40	4.50	10.51

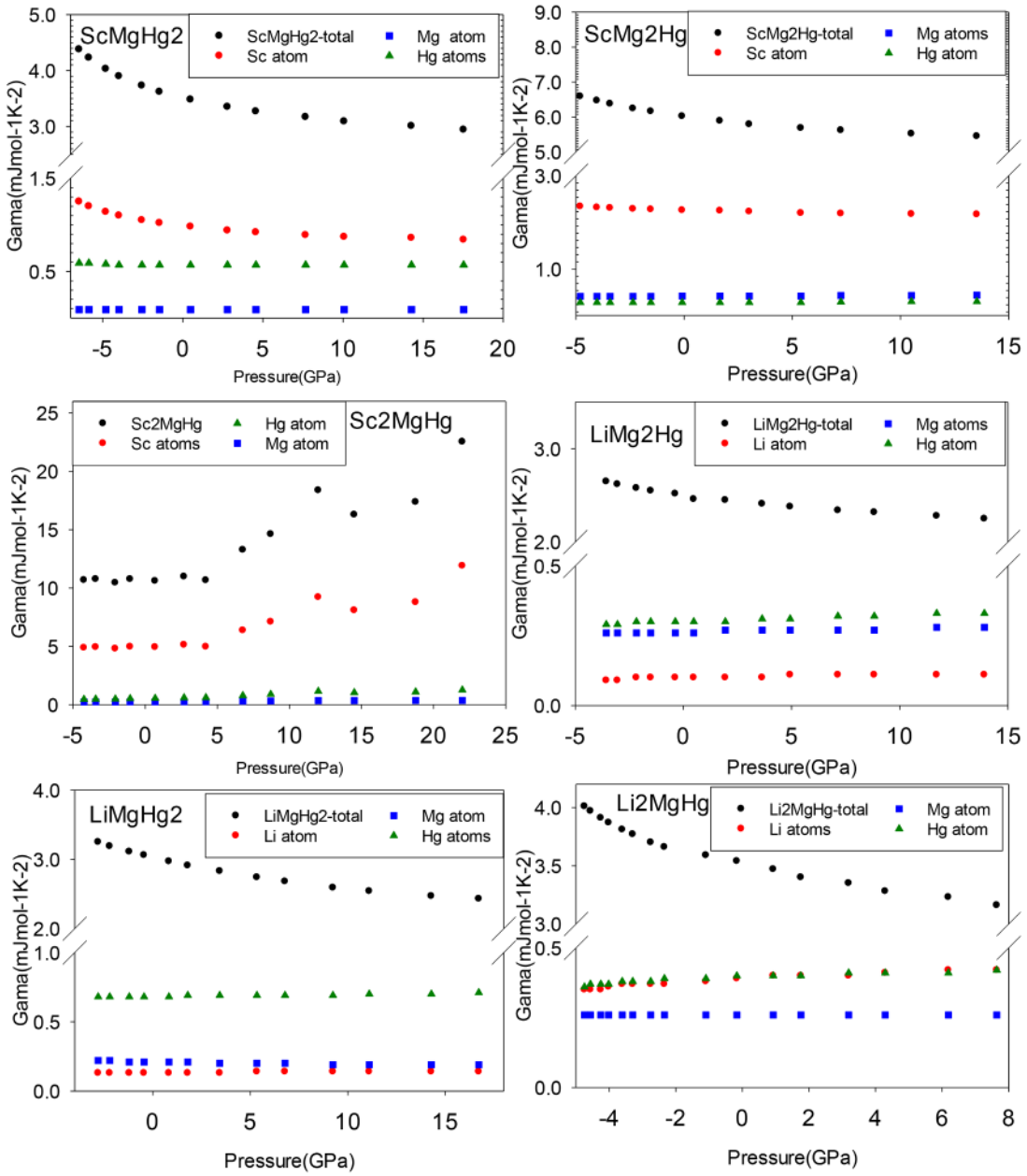

Fig. 7. The total and partial contributions of Sc, Li, Mg, and Hg atoms to the linear electronic specific heat within mBJ approach in the presence of spin-orbit interaction at different pressures.

with space group $F\bar{4}3m(216)$, while the other compounds are more stable in the cubic structure with space group $Fm\bar{3}m$ (225). Additionally, the calculated phonon dispersion shows that XMg_2Hg, $XMgHg_2$, and X_2MgHg (X = Sc and Li) compounds, except for Li_2MgHg in the $Fm\bar{3}m$ crystal structure and Sc_2MgHg and $LiMg_2Hg$ compounds in $F\bar{4}3m$ crystal structure, are dynamically stable. In contrast, $ScMg_2Hg$ and Li_2MgHg compounds in the $F\bar{4}3m$ crystal structure are dynamically unstable.

The calculated elastic constants satisfy the Born-Huang criteria, confirming the mechanical stability of these materials. The bulk modulus, shear modulus, and Young's modulus were determined, showing that Sc-based compounds are stiffer and less compressible compared to Li-based compounds. Sc_2MgHg and Li_2MgHg exhibit the highest and lowest stiffness, respectively. The ductility and brittleness were assessed using Poisson's ratio and Pugh's ratio, revealing that $ScMgHg_2$ and $ScMg_2Hg$ are ductile, whereas the other compounds are brittle. The interatomic forces in $ScMg_2Hg$, $ScMgHg_2$, and $LiMg_2Hg$ are predominantly ionic, as indicated by their Poisson's ratios. The positive Cauchy pressure values confirm metallic-like bonding in these compounds. Elastic anisotropy calculations reveal that $ScMg_2Hg$ has more pronounced anisotropy compared to $ScMgHg_2$.

The electronic properties were analyzed through the density of states and band structure calculations. All compounds were found to be metallic, with significant contributions to the electron density of states at the Fermi energy primarily from Mg atoms. The linear electronic specific heat of Sc-based compounds is higher than that of Li-based compounds. The band structures revealed notable features, such as flat electron bands and a Dirac point at the Gamma point for $ScMgHg_2$. The pressure dependence of the electronic specific heat and band structures indicated no topological phase transitions, confirming that these compounds are normal metals.

This comprehensive study enhances our understanding of the structural, mechanical, and electronic behaviors of these full-Heusler compounds, laying the groundwork for future material design and

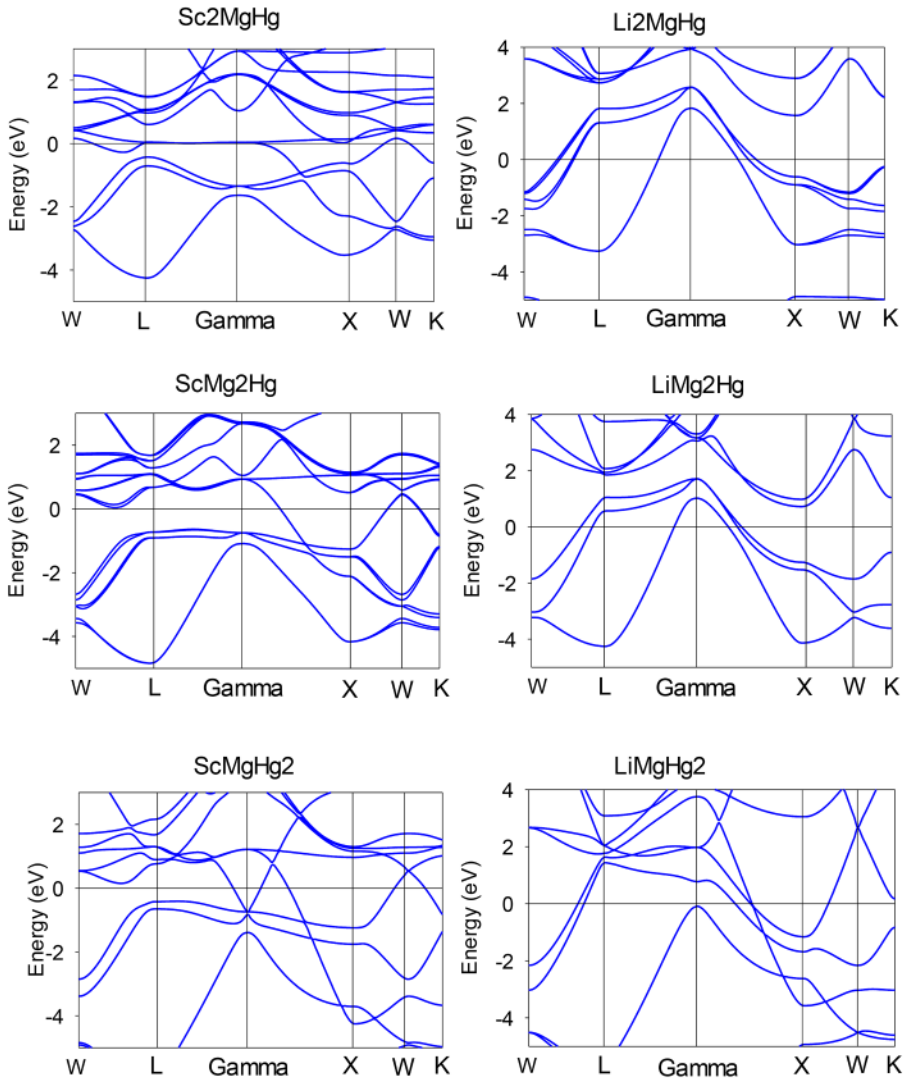

Fig. 8. The calculated band structure of XMg_2Hg, $XMgHg_2$, and X_2MgHg (X = Sc and Li) compounds using the within mBJ approach in the presence of spin-orbit interaction.

applications in advanced technologies.

CRediT authorship contribution statement

Salman Alsaedi: Writing – original draft, Visualization, Validation, Software, Methodology, Investigation, Formal analysis, Data curation. **Zahra Nourbakhsh:** Writing – review & editing, Validation, Supervision, Software, Resources, Project administration, Methodology, Investigation, Funding acquisition, Formal analysis, Conceptualization. **Aminollah Vaez:** Writing – review & editing, Validation, Supervision, Project administration, Methodology, Investigation, Formal analysis. **Daryoosh Vashaee:** Writing – review & editing, Validation, Supervision, Investigation, Funding acquisition, Formal analysis.

Declaration of competing interest

The authors declare that they have no known competing financial interests or personal relationships that could have appeared to influence the work reported in this paper.

Data availability

Data will be made available on request.

Acknowledgment

DV acknowledges funding support from the National Science Foundation (NSF) under grant number CBET-2110603.

References

[1] https://next-gen.materialsproject.org.
[2] Timotheus Hohl, Frank Tambornino, Constantin Hoch, Structure and bonding in CsNa2Hg18, a new ternary amalgam with strong coulombic bonding contributions, Crystals. 12 (2022) 1679, https://doi.org/10.3390/cryst12111679.
[3] Andriy V. Tkachuk, Arthur Mar, Li6A17Hg9 (A=Ca, Sr, Yb): intermetallic compounds of mercury with a zeolite-like topology of cubic networks, Chem.–A Euro. J. 15 (2009) 10348–10351, https://doi.org/10.1002/chem.200902250.
[4] H. Pauly, A. Weiss, H. Witte, Kubisch flächenzentrierte Legierungen der Zusammensetzung Li2MsX mit raumzentrierter Unterstruktur, Internat. J. Mater. Res. 59 (5) (1968) 414–418, https://doi.org/10.1515/ijmr-1968-590512.
[5] Kristian Berland, Ole Martin Løvvik, Rasmus Tranås, Discarded gems: thermoelectric performance of materials with band gap emerging at the hybrid-functional level, Appl. Phys. Lett. 119 (2021) 081902, https://doi.org/10.1063/5.0058685.
[6] J. Wang, J. Mark, K. Woo, J. Voyles, K. Kovnir, Chemical flexibility of Mg in Pnictide materials: structure and properties diversity, Chem. Mater. 31 (20) (2019) 8286–8300, https://doi.org/10.1021/acs.chemmater.9b03740.
[7] X-F. Wang, J-W. Yang, "Ab initio investigations of electronic structure, mechanical properties, phonon stability, and thermodynamics of the Mg–Er system", 2022. 199, 110968 10.1016/j.vacuum.2022.110968.

[8] A. Ayuela, J. Enkovaara, K. Ullakko, R.M. Nieminen, Structural properties of magnetic Heusler alloys, J. Phys. 11 (8) (1999) 2017, https://doi.org/10.1088/0953-8984/11/8/014.

[9] B. Karki, G. Ackland, J. Crain, Elastic instabilities in crystals from ab initio stress-strain relations, J. Phys. 9 (41) (1997) 8579, https://doi.org/10.1088/0953-8984/9/41/005.

[10] M.E. Fine, L.D. Brown, H.L. Marcus, Elastic constants versus melting temperature in metals, Scripta metallurgica 18 (9) (1984) 951–956, https://doi.org/10.1016/0036-9748(84)90267-9.

[11] J.J. Gilman, Electronic basis of the strength of materials, Cambridge University Press, 2003.

[12] Shu-Chun Wu, Gerhard H. Fecher, S. Shahab Naghavi, Claudia Felser, Elastic properties and stability of Heusler compounds: Cubic Co2YZ compounds with L21 structure, J. Appl. Phys. 125 (8) (2019) 082523, https://doi.org/10.1063/1.5054398.

[13] K. Schwarz, P. Blaha, G.K.H. Madsen, Electronic structure calculations of solids using the WIEN2k package for material sciences, Comput. Phys. 147 (2002) 71–76, https://doi.org/10.1016/S0010-4655(02)00206-0.

[14] P. Blaha, K. Schwarz, G.K.H. Madsen, D. Kvasnicka, J. Luitz, wien2k: An augmented plane wave+local orbitals program for calculating crystal properties, Vienna University of Technology, Austria, 2010. http://www.wien2k.at/reg_user/textbooks/usersguide.pdf.

[15] J.P. Perdew, K. Burke, M. Ernzerhof, Generalized gradient approximation made simple, Phys. Rev. Lett. 77 (1996) 3865, https://doi.org/10.1103/PhysRevLett.77.3865.

[16] E. Engel, S.H. Vosko, Fourth-order gradient corrections to the exchange-only energy functional: Importance of∇ 2 n contributions, Phys. Rev. B 50 (1994) 10498, https://doi.org/10.1103/PhysRevB.50.10498.

[17] D. Koller, F. Tran, P. Blaha, Improving the modified Becke-Johnson exchange potential, Physic. Rev. B 85 (15) (2012) 155109, https://doi.org/10.1103/PhysRevB.85.155109.

[18] W. Bao, L. Dan, L. Ping, D. Yonghua, Structural properties, elastic anisotropies and thermal conductivities of tetragonal LnB_2C_2 (Ln= Rare Earth) compounds from first-principles calculations, Ceram. Int. 45 (2) (2019) 1857–1867, https://doi.org/10.1016/j.ceramint.2018.10.077.

[19] M. Jamal, M. Bilal, Iftikhar Ahmad, S. Jalali-Asadabadi, IRelast package, J. Alloys. Compd. 735 (2018) 569–579, https://doi.org/10.1016/j.jallcom.2017.10.139.

[20] M. Born, On the stability of crystal lattices. I, in: Mathematical proceedings of the cambridge philosophical society 36, Cambridge University Press, 1940, pp. 160–172, https://doi.org/10.1017/S0305004100017138.

[21] S. Yalameha, Z. Nourbakhsh, D. Vashaee, ElATools: A tool for analyzing anisotropic elastic properties of the 2D and 3D materials, Comput. Phys. Commun. 271 (2021) 108195, https://doi.org/10.1016/j.cpc.2021.108195.

[22] W. Voigt, Lehrbuch der kristallphysik:(mit ausschluss der kristalloptik), 962, Teubner Leipzig, 1928. https://scholar.google.com/. scholar?q=%22W.±Voigt,±1910.±Lehrbuch±der±kristallphysik&hl=en&as_sdt=0&as_vis=1&oi=scholart.

[23] A. Reuss, Berechnung der Fließgrenze von Mischkristallen auf Grund der Plastizitätsbedingung für Einkristalle, J. Appl. Math. Mech. 9 (1929) 49, https://doi.org/10.1002/zamm.19290090104.

[24] J. Wang, J. Wang, Y. Zhou, C. Hu, Phase stability, electronic structure and mechanical properties of ternary-layered carbide Nb4AlC3: An ab initio study, Acta Mater. 56 (2008) 1511–1518, https://doi.org/10.1016/j.actamat.2007.12.003.

[25] R. Li, Q. Shao, E. Gao, Z. Liu, Elastic anisotropy measure for two-dimensional crystals, Extreme Mech. Lett. 34 (2020) 100615, https://doi.org/10.1016/j.eml.2019.100615.

[26] C.M. Zener, S. Siegel, Elasticity and Anelasticity of Metals, J. Phys. Chem. 53 (9) (1949) 1468, https://doi.org/10.1021/j150474a017. -1468.

[27] C.M. Kube, Elastic anisotropy of crystals, AIP. Adv. 6 (2016) 095209, https://doi.org/10.1063/1.4962996.

[28] H. Ma, X.D. Zhang, F. Wang, First-principles study of the lattice vibration, elastic anisotropy and thermodynamical properties of Tantalum Silicide with the different crystal structures, Vacuum. 191 (2021) 110410.

[29] A. Togo, I. Tanaka, First principles phonon calculations"in materials science, Scr. Mater. 108 (2015) 1–5, https://doi.org/10.1016/j.scriptamat.2015.07.021.

[30] S. Ryan Kingsbury, Andrew S. Rosen, Ayush S. Gupta, Jason M. Munro, Shyue Ping Ong, Anubhav Jain, Shyam Dwaraknath, Matthew K. Horton, Kristin A. Persson, A flexible and scalable scheme for mixing computed formation energies from different levels of theory, NPJ. Comput. Mater. 8 (2022) 195, https://doi.org/10.1038/s41524-022-00881-w.

[31] L.I. Tenelanda-Osorio, M.E. Vélez, First principles study of the thermodynamic, mechanical and electronic properties of crystalline phases of Chromium Nitrides, J. Phys. Chem. Solids 148 (2021) 109692, https://doi.org/10.1016/j.jpcs.2020.109692.

[32] M. De Jong, W. Chen, T. Angsten, A. Jain, R. Notestine, A. Gamst, M. Sluiter, C. Krishna Ande, S. Van Der Zwaag, J.J. Plata, C. Toher, Charting the complete elastic properties of inorganic crystalline compounds, Sci. Data 2 (1) (2015) 1–13, https://doi.org/10.1038/sdata.2015.9.

[33] W. Bao, Li. Dan, L. Ping, D. Yonghua, Elastic anisotropies and thermal properties of cubic TMIr (TM= Sc, Y, Lu, Ti, Zr and Hf): A DFT calculation, Mater. Res. Express. 6 (8) (2019) 086574, https://doi.org/10.1088/2053-1591/ab1f01.

[34] X.Zhang K.Wang, F. Wang, Exploring the electronic, mechanical, anisotropic and optical properties of the Sc-Al-C MAX phases from a first principles calculations, Chem. Phys. Lett. 836 (2024) 141024, https://doi.org/10.1016/j.cplett.2023.141024.

[35] https://www.engineeringtoolbox.com.

[36] M. Tian, X. Zhang, F. Wang, Structural, mechanical, electronic and thermodynamic properties of YBC, YB_2C, YB_2C_2, $Y_2B_3C_2$ intermetallics, Mater. Today Commun. 39 (2024) 108696, https://doi.org/10.1016/j.mtcomm.2024.108696.

[37] D.G. Pettifor, Theoretical predictions of structure and related properties of intermetallics, Materials, Sci. Techn. 8 (2013) 345–349, https://doi.org/10.1179/mst.1992.8.4.345.

[38] D. Nguyen-Maxh, D.G. Pettifor, S. Znam, V. Vitek, Negative Cauchy pressure within the tight-binding approximation, MRS Online Proceed. Library (OPL) 491 (1997) 353, https://doi.org/10.1557/PROC-491-353.

[39] D. Qu, C. Li, L. Bao, Z. Kong, Y. Duan, First-principles predictions of electronic, elastic, and optical properties of ScBC and YBC ternary cermet phases, J. Phys. Chem. Solids 138 (2020) 109253, https://doi.org/10.1016/j.vacuum.2020.109488.

[40] Y. Duan, Y. Wang, M. Peng, K. Wang, Insight into anisotropies in mechanical and thermal properties of $AGdS_2$ (A = alkali metals) ternary gadolinium sulfides", Mater. Today Commun. 26 (2021) 101991 https://doi.org/10.1016/j.mtcomm.2020.101991.

[41] C. Li, X. Zhang, F. Wang, Influence of TM elements on the mechanical and thermodynamic properties of Hf2Si intermetallics, Volume 220, 2024, 112793 10.1016/j.vacuum.2023.112793.

[42] Kelvin Elphick, William Frost, Marjan Samiepour, Takahide Kubota, Koki Takanashi, Hiroaki Sukegawa, Seiji Mitani, Atsufumi Hirohata, Heusler alloys for spintronic devices: review on recent development and future perspectives, Sci. Technol. Adv. Mater. 22 (1) (2021) 235–271.

[43] Yan Yang, Xiaoming Xiong, Jing Chen, Xiaodong Peng, Daolun Chen, Fusheng Pan, Research advances in magnesium and magnesium alloys worldwide in 2020, J. Magn. Alloys 9 (3) (2021) 705–747.

[44] Jason K. Kawasaki, Shouvik Chatterjee, Paul C. Canfield, Guest Editors, Full and half-Heusler compounds, MRS Bull. 47 (6) (2022) 555–558.

[45] Jovan Tan, Seeram Ramakrishna, Applications of magnesium and its alloys: A review, Appl. Sci. 11 (15) (2021) 6861.